# ChemComm

## Accepted Manuscript

This article can be cited before page numbers have been issued, to do this please use: R. Tan, J. Yang, J. Hu, K. Wang, Y. Zhao and F. Pan, *Chem. Commun.*, 2015, DOI: 10.1039/C5CC08002A.

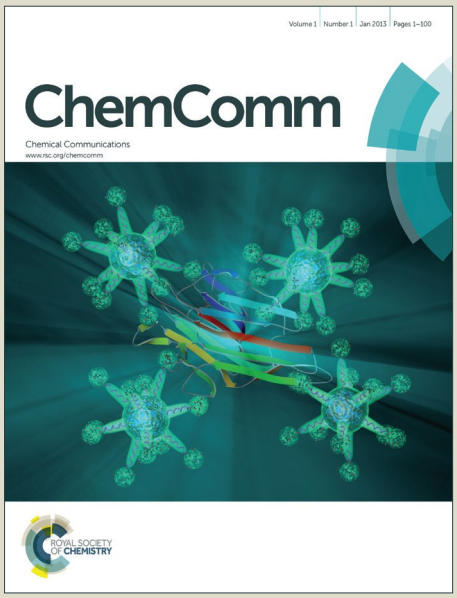


This is an *Accepted Manuscript*, which has been through the Royal Society of Chemistry peer review process and has been accepted for publication.

*Accepted Manuscripts* are published online shortly after acceptance, before technical editing, formatting and proof reading. Using this free service, authors can make their results available to the community, in citable form, before we publish the edited article. We will replace this *Accepted Manuscript* with the edited and formatted *Advance Article* as soon as it is available.

You can find more information about *Accepted Manuscripts* in the Information for Authors.

Please note that technical editing may introduce minor changes to the text and/or graphics, which may alter content. The journal's standard Terms & Conditions and the Ethical guidelines still apply. In no event shall the Royal Society of Chemistry be held responsible for any errors or omissions in this *Accepted Manuscript* or any consequences arising from the use of any information it contains.

ROYAL SOCIETY OF CHEMISTRY

www.rsc.org/chemcomm

View Article Online
DOI: 10.1039/C5CC08002A

Journal Name

COMMUNICATION

# Core-shell nano-$FeS_2$@N-doped graphene as advanced cathode material for rechargeable Li-ion batteries

Received 00th January 20xx,
Accepted 00th January 20xx

DOI: 10.1039/x0xx00000x

www.rsc.org/

Rui Tan[+], Jinlong Yang[+], Jiangtao Hu[+], Kai Wang, Yan Zhao and Feng Pan[*]

**We report the formation of core-shell nano-$FeS_2$@N-doped graphene as a novel cathode material and its mechanism for rechargeable Li-ion batteries. Benefit of the amount of $FeS_2$ nano-crystals as the core for Li-ion storage with high capacity and coated N-doped graphene as the shell with excellent electron conduction to enhance the structure stability, $FeS_2$@N-graphene exhibits more remarkable specific energy (950 Wh $kg^{-1}$ at 0.15 kW $g^{-1}$) and higher specific power (543 Wh $kg^{-1}$ at 2.79 kW $g^{-1}$) than the commercial rechargeable LIB cathodes, as well as stable cycling performance (~600 Wh $kg^{-1}$ at 0.75 kW $g^{-1}$ after 400 cycles).**

Rechargeable Li-ion cells play a pivotal role in energy storage and electronic devices. However due to the energy density of commercial cathode materials (including $LiCoO_2$, $LiNi_{0.5}Co_{0.2}Mn_{0.3}O_2$, $LiMn_2O_4$, $LiFePO_4$, etc.) for Li-ion battery approaching a upper limit, next generation cathodes need to be developed to satisfy the increased demand for advanced Li-ion cells.[1-4]

Among the advanced electrode materials based on metal sulfide,[5-8] pyrite $FeS_2$ is an interesting cathode material for a new type of Li-ion battery, which has lots of advantages such as high theoretical capacity, good thermal stability, abundance in nature, environmental benignity and safety. By reaction with four Li-ions, Pyrite $FeS_2$ can provide 890 mAh $g^{-1}$ ($FeS_2+4Li^++4e^-\rightarrow Fe+2Li_2S$), which is about 5 times of the specific capacity of $LiFePO_4$ (170 mAh $g^{-1}$) . Based on the advantage of remarkable high capacity of Li-ion storage, currently, Pyrite $FeS_2$ has been widely utilized in commercial primary batteries and shows remarkable electrochemical performance[9]. Recently, pyrite $FeS_2$ has been investigated as secondary Li-ion cells cathodes or anodes.[10,11]

However, the main problems associated with $FeS_2$ applying in rechargeable Li-ion cells include the polysulfide dissolution in electrolyte, low conductivity and large volume expansion. The mechanism of the performance of pyrite $FeS_2$ is still a controversial subject. $FeS_2$, $FeS_x$ and S have been thought as main products during the charge process by former reports[12,13], of which $Li_2S_x$ ($2\leq x\leq 8$) may be formed during the charging-discharging procedure and can dissolve in the electrolyte to lead to unfavorable side reactions with lithium metal. Owing to these reasons, the reported rechargeable cells with $FeS_2$, currently, have low coulombic efficiency and degrades quickly. In order to improve the performance of $FeS_2$ cells, numerous approaches have been tried, such as modifying the particle surface by conductive materials to enhance the electronic conductivity[14,15], downsizing the size and changing shapes of pyrite $FeS_2$ to shorten the Li-ionic transfer length[16], utilizing all-solid-state electrolytes[17] and optimizing polymer electrolyte[18-20] to prevent unfavorable shuttle effects of intermediate sulfur at working time and so on. In former studies, the cells with carbon-coated $FeS_2$ have good performance and long-term stability at high current rate, indicating the low cost carbon-coated pyrite $FeS_2$ is a promising candidate for commercial Li-ion batteries. For instance Yan Yu group[21] developed a facile way to prepare $FeS_2$@porous C-nanooctahedra, which exhibits superior rate capability (at 5 C, 256 mAh $g^{-1}$ obtained) and stable cycling performance (at 0.5 C, 495 mAh $g^{-1}$ obtained after 50 cycles). Se-Hee Lee group[22] used polyacrylonitrile (PAN) matrix to modify the $FeS_2$ surface and to accommodate the volume expansion of $FeS_2$ during the charging-discharging procedure. Due to the low conductivity of PAN matrix, the specific capacity of $FeS_2$@PAN is still low. The composite of $FeS_2$ microspheres@reduced graphene oxide has been studied as Li-ion cell anodes by Chun-Sing Lee group, which show high capacity and long life performance, of which 380 mAh $g^{-1}$ has been obtained at 10 C (8.9 A $g^{-1}$) over 2000 cycles.[11] In addition, doping of the heteroatoms (N, S, P, B, etc.) in the graphene shell[23-25] can improve its conductivity,which can be proposal to further optimize the electrochemical performance for pyrite $FeS_2$.

Herein, we for the first time report a facile and novel method to prepare pyrite nano-$FeS_2$ wrapped in the N-graphene frameworks (core-shell nano-$FeS_2$@N-graphene). Owing to nano-size $FeS_2$ with short Li-ionic diffusion distance, N-graphene shell with optimized electronic conductivity to enhance the structure stability, as well as N-graphene frameworks between the nanoparticles possessing more fast charge transfer channels to reduce the resistance, the pyrite $FeS_2$ cells with LiTFSI/DOL/DME/$LiNO_3$ have superior electrochemical performances with high reversible capacity of 484.7 mAh $g^{-1}$ at 0.5 A $g^{-1}$ corresponding to specific capacity of 713.49 Wh $kg^{-1}$ and the fast rechargeable performance of 281.4 mAh $g^{-1}$ (543 Wh $kg^{-1}$) at 5 A $g^{-1}$ at room temperature. Additionally, the cells with core-shell nano-$FeS_2$@N-graphene cathode have excellent long-term stability and high specific energy,

*School of Advanced Materials, Peking University, Peking University Shenzhen Graduate School, Shenzhen 518055, China. Tel: 86-755-26033200; E-mail: panfeng@pkusz.edu.cn.*

† Electronic Supplementary Information (ESI) available: [experimental procedures, theoretical details, figures and tables.] See DOI: 10.1039/x0xx00000x

View Article Online
DOI: 10.1039/C5CC08002A




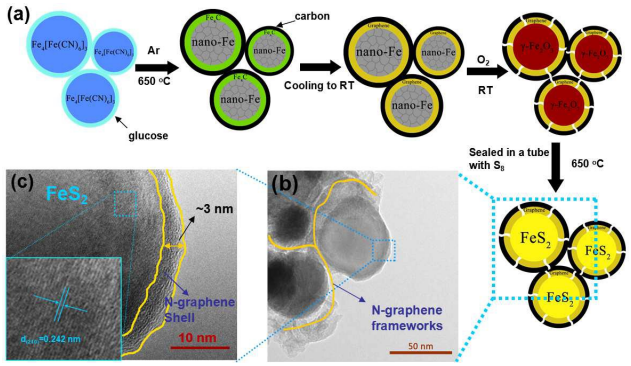


**Fig. 1** (a) Brief illustration of the fabrication of $FeS_2$@N-graphene (RT: room temperature), (b) TEM image of $FeS_2$@N-graphene particles, (c) high-resolution TEM image of $FeS_2$@N-graphene particles (inset shows the (210) planes of pyrite $FeS_2$ with interlayer distances 0.242 nm).

containing 401.1 mAh $g^{-1}$ (613.7 Wh $kg^{-1}$) at 0.5 A $g^{-1}$ after 400 cycles, which is higher than the commercial rechargeable Li-ion battery and also better stability than that of most of reported $FeS_2$ battery.

The preparation scheme and basic characteristics of as synthesized core-shell $FeS_2$@N-graphene are shown in **Fig. 1** and **Fig. 2**. **Fig. 1a** briefly illustrates the synthesis process. In our previous work[26], when Prussian blue precursors were calcined at argon atmosphere, nano-Fe and $Fe_xC$ were produced by reduction with glucose, and then carbon layers were attached to $Fe_xC$ to generate a shell structure. When cooled down and exposed in the air, the core-shell γ-$Fe_2O_3$@N-graphene formed. Hereafter, core-shell γ-$Fe_2O_3$@N-graphene (SEM and TEM images seen in the **Fig. S1**) was used as an important intermediate template to form core-shell $FeS_2$@N-graphene particles by sealing γ-$Fe_2O_3$@N-graphene and sulfur in a small tube with the thermal process (see **Fig. S2**). The tap density of obtained $FeS_2$@N-graphene is ~1.2 g $cm^{-3}$, comparable to the commercial $LiFePO_4$.

To attest the shell with N-doped graphene, element mapping are shown in **Fig. 2c** and **Fig.S3**. Nitrogen element (pink) is combined with the $FeS_2$ (blue and green). Considering the low content of nitrogen and instrumental errors, XPS were carried out (**Fig. 2d**). The high resolution N1s XPS spectrum of $FeS_2$@N-graphene of $FeS_2$@N-graphene can be fitted into three main peaks (at 398.2, 400.2 and 401.3 eV). The peaks at low binding energy 398.2 and 400.2 eV correspond to pyridinic N and pyrrolic N respectively. And the peak at high binding energy 400.8~401.3 eV means that carbon atoms within carbon layers are substituded by nitrogen atoms in form of graphic N.[27-30] The high resolution $C_{1s}$ banding energy can be fitted into four components, corresponding to carbon atoms in five different chemical environmental (**Fig. S4c**): $C_{sp^2}$ (284.49 eV), $C_{sp^3}$ (285.2 eV), C-O (286.2 eV) and C=O (289.4 eV). The percentage of $C_{sp^2}$ is 68.55, demonstrating the carbon shell owns high graphitization degree. In order to understand more details about the graphene shell, shell materials were identified by HRTEM image (**Fig. S4a**) and Raman spectrum (**Fig. S4b**). A large number of graphene layers were observed in Fig.S4a and the 2D peak at 2700 $cm^{-1}$ confirmed the graphene layer structure. Based on the reported works[23,24], N-doped graphene can further improve its conductivity and further improve electrochemical performances of pyrite $FeS_2$ with poor conductivity. Meanwhile the thermal stability measured by TG seen in **Fig. S5** shows that $FeS_2$@N-graphene is stable at high temperature (decomposition at ~300 °C).

Inset of **Fig. 2c** shows the core-shell of nano-$FeS_2$@N-graphene to aggregate as micron particles to share with boundary of N-graphene. Li-ion electrode materials with micron dimensions can take advantage of high volumetric specific energy and facile processability for practical applications. Observing from **Fig. 2a**, the prime $FeS_2$ (red) particle with 50~100 nm were closely wrapped in the N-doped graphene frameworks (blue). The XRD pattern (**Fig. 2b**) with well-defined diffraction peaks also proves the nano-$FeS_2$ with the cubic structure (JCPDF card No. 42-1340, space group $Pa\bar{3}$, a=5.419 Å) without other infaust impurities like marcasite, greigite, pyrrhotite or sulfur. But because of utilizing glass tubes in the synthesis process, inevitable impurities with very little content occur. The average particle sizes are approximately 50 nm measured by XRD with calculation according to the Scherrer formula, which is corelated to amont of prime $FeS_2$ nano-crystals in the core-shell mearsured by TEM in **Fig. 2a**.

In this structure, nano sized $FeS_2$ has short Li-ionic diffusion distance while N-graphene frameworks with optimized electronic conductivity can supply more contact area to reduce resistance, which means charge transfer channels are created around particles. In order to obtain more detailed observations of the N-graphene frameworks connected to single prime $FeS_2$, the suface states of $FeS_2$ were investigated by TEM (**Fig. 1b**) and HRTEM (**Fig. 1c**). Besides the N-graphene frameworks, the N-graphene shells with about 3 nm thickness tightly attached to $FeS_2$. Advantage of the shell structure with excellent electronic conductivity can both improve the low conductive surface of $FeS_2$ as well as enhance the structural stability due to volume change in the charge-discharge process. Therefore, combination with advantages of short Li-ionic distance of nano-size $FeS_2$, the structure stability enhanced by N-graphene shell and fast charge transfer paths around N-graphene frameworks lead to the superior electrochemical performances of core-shell nano-$FeS_2$@N-graphene for Li-ion battery as below.

The Li-ion storage performances of as-synthesis nano-$FeS_2$@N-graphene were studied by cyclic voltammetry (CV) and electrochemical properties using two-electrode coin cells. **Fig.3a** shows the first four CV curves of nano-$FeS_2$@N-graphene for Li-ion cells with 1 M LiTFSI and 0.3 M $LiNO_3$ in DOL/DME at a scanning rate of 0.2 mV $s^{-1}$. For the first cycle, two wide reduction peaks (at approximate 1.48 and 1.22 V) and two oxidation reduction peaks (1.89 and 2.61 V) were seen. The reduction peaks at ~1.48 and 1.22 V attribute to the decomposition of $LiNO_3$[31] (providing large irreversible capacity), and reduction of nano-$FeS_2$, which are corresponding to the voltage platform at the 1st cycle curve in **Fig.S6**. From the first five CV curves of Li-ion cells without $LiNO_3$ were shown in Fig. S6, a single

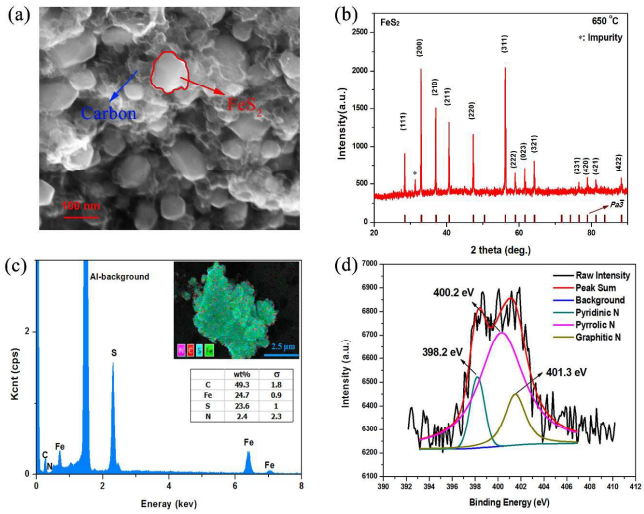


**Fig. 2** Basic characteristics of the as-synthesized $FeS_2$@N-graphene particles: (a) SEM image of $FeS_2$ particles (red) and carbon regions (blue), (b) XRD patterns, (c) EDX image, (d) binding energy of N1s in $FeS_2$@N-graphene sample.

View Article Online
DOI: 10.1039/C5CC08002A




reduction peak was shown at approximate 1.3 V, attributing to the following reactions[18, 21, 22]:

$$FeS_2 + 2Li^+ + 2e^- \rightarrow Li_2FeS_2 \quad (1)$$

$$Li_2FeS_2 + 2Li^+ + 2e^- \rightarrow Li_2S + Fe \quad (2)$$

Around room temperature (~30 °C), these two reactions proceed synchronously due to the slow diffusion of Li-ion into pyrite, explaining the single platform at about ~1.4 V in the **Fig. S7**. From the second cycle onwards, there is a slight change at about 1.99 and 2.20 V reflecting new reactions proceeding. Combining with the CV analysis and XRD patterns at different charge/discharge state (**Fig. S8**), the reversible reaction mechanism and phase transformation were illustrated in Fig.3c and 3d with the phase structure vs. electrochemical performance during the charge-discharge process with different "State" (State 1-4). According to the previous studies[12,13], the charging steps may attribute to the following reactions:

$$Li_2S + Fe \rightarrow Li_2FeS_2 + 2Li^+ + 2e^- \quad (3)$$

$$Li_2FeS_2 \rightarrow Li_{2-x}FeS_2 + xLi^+ + xe^- \ (0.5 \le x \le 0.8) \quad (4)$$

$$Li_{2-x}FeS_2 \rightarrow FeS_y + (2-y)S + (2-x)Li^+ + (2-x)e^- \ (0.8 < x \le 2) \quad (5)$$

As cycle number increased, the redox reaction voltages are nearly unchanged, reflecting good reversibility of nano-$FeS_2$@N-graphene. The typical cycling curves in **Fig.3b** and **4b** show that the capacity of cells decays very slowly with ~0.9 mAh $g^{-1}$ per cycle from 2nd to 400th cycle at 0.5 A $g^{-1}$.

During the discharing procedure (**Fig.3c-d**), $FeS_y$ (y≤2, State 3) transforms to $Li_2FeS_2$ (State 2) and then to Fe and $Li_2S$ (state 1), of which Fe can form a conductive framework to promote the reversible reaction of $Li_2S$. During the charing procedure, theoretically, the iron is oxidated to provide electron to react with $Li_2S$ to form $Li_2FeS_2$, then further to form $FeS_y$ in the charging. Actually, in the initial stage of $Li^+$ extraction, iron can react with $Li_2S$ to form $Li_2FeS_2$ at the interface between the Fe nano-particle and $Li_2S$ (State 1 in Fig. 3c-d) until the whole iron and $Li_2S$ transform into $Li_2FeS_2$ (State 1 to 2.1 in Fig. 3c-d). In this case, downsized particles wrapped in conductive frameworks have the shorter $Li^+$ diffusion distance and more electron tranfer channels, due to which the reversible redox can proceed with fast kinetics. With the number of extracted Li-ions increased, $Li_2FeS_2$ starts to supply Li-ions and electrons to form $Li_{2-x}FeS_2$ (State 2 to 3, in Fig.3c-d). Note that the intermediate structure of $Li_{2-x}FeS_2$ is unstable and changeable, which directly affects the transfer ability of Li-ions. Two kinds of $Li^+$ in $LiS_4$ with tetrahedron structure and $LiS_6$ with octahedron structure, respectively, co-

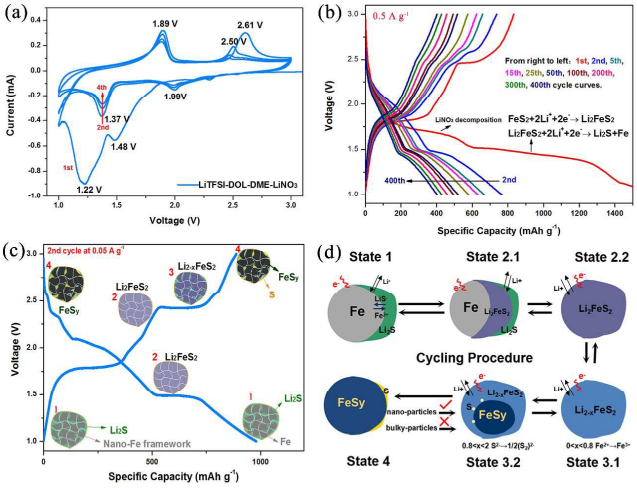


**Fig.3** Electrochemical performances of assembled cells with $FeS_2$@N-graphene particles: (a) cyclic voltammetry curves (from 1st to 4th cycle at 0.2 mV $s^{-1}$), (b) cycling curves from 2nd to 100th cycle at 0.5 A $g^{-1}$, (c-d) schematic diagram for reation mechanism.

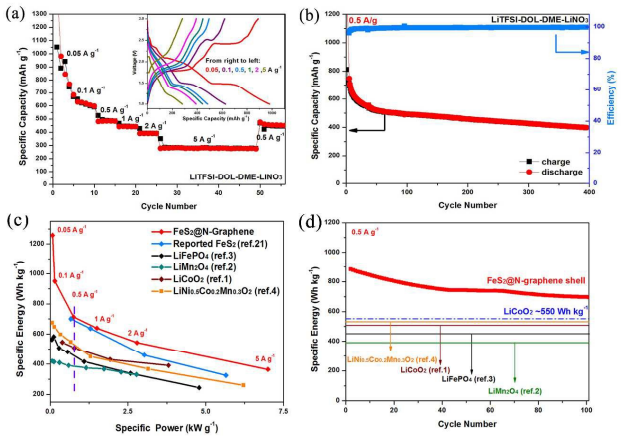


**Fig.4** (a) Rate performances of cells at 0.05, 0.1, 0.5, 1, 2, 5 A $g^{-1}$ (Inset is the typical charging-discharging curves), (b) long cycling performance from 2nd to 400th cycle at 0.5 A $g^{-1}$. (c) discharge energy density of $FeS_2$@N-graphene particles compared to other commercial Li-ion cell cathode materials. (d) discharge energy density of $FeS_2$@N-graphene particles vs. cycle number shown at 0.5 A $g^{-1}$ along with the theoretical discharge specific energy of $LiCoO_2$ (~550 Wh $kg^{-1}$, which is calculated using an average voltage of 3.9 V and a specific capacity of 140 mAh $g^{-1}$) and the energy density of $LiCoO_2$, $LiFePO_4$, $LiMn_2O_4$, $LiNi_{0.5}Co_{0.2}Mn_{0.3}O_4$, at 0.5 A $g^{-1}$.

exist in $Li_{2-x}FeS_2$ structure.[32-34] When 0<x<0.8 in $Li_{2-x}FeS_2$, tetrahedral $Li^+$ ions start to be extracted and $Fe^{2+}$ changes to $Fe^{3+}$ shown in the State 3.1 of Fig. 3d. During such period, $Li^+$ and $e^-$ can transfer smoothly due to the stable $Li_{2-x}FeS_2$ structure with $LiS_6$ octahedron. However, while the content of tetrahedral $Li^+$ ions decrease to low ratio, $S^{2-}$ oxidation reaction ($S^{2-} \rightarrow 1/2(S_2)^{2-}$) happens and octahedral $Li^+$ ions transfer increase, directly resulting in the huge volume change of $Li_{2-x}FeS_2$ structure. $Li^+$ extraction from these intermediate structures are difficult with high polarization due to the low electronic conductivity, which cause that some part of $(S_2)^{2-}$ is overcharged to form sulfur nano-particles shown in State 3.2 of Fig.3d. With the x in $Li_{2-x}FeS_2$ increasing (x from 0 to 1.5) , the $Li^+$ diffusivity decrease from 5.0 × $10^{-8}$ cm $s^{-1}$ to 2 ×$10^{-9}$ cm $s^{-1}$.[33] It's worth to predict that if the size of $FeS_2$ particles becomes smaller and the electronic conductivity of $FeS_2$ particles gets better, the Li-ions and electrons are easier to extract from $Li_{2-x}FeS_2$ due to the shorter Li-ionic diffusion distance and better electronic conductivity, so that shutter reaction due to $Li_2S_x$ (2≤x≤8) and generation of S nano-particles may avoid because $S^{2-}$ prefer to form $(S_2)^{2-}$ to combine with $Fe^{3+}$ (from state 3.2 to 4 in Fig. 3c-d). S nano-particles are always generated in general cases to have low dissolution ability in electrolyte[35]. Besides downsizing the $FeS_2$ particle to shorten the $Li^+$ diffusion distance, $LiNO_3$ play a very essential role in alleviating parasitic reactions between Li metal and already present sulfur species to optimize cycling the performance of $FeS_2$ based Li-ion batteries. Mechanism with $LiNO_3$ doping was proposed that $LiNO_3$ can be directly reduced by lithium to $Li_xNO_y$ and oxidized by sulfur species to $Li_xSO_y$, forming a Li-N-S-O passivating layer coating upon the lithium anodes[20]. In this work, it can be observed that the surface of Li anode is not smooth with dark species formed on the lithium, e.g. such as the SEM images of lithium anode surfaces after discharging shown in **Fig. S9**. Additionally, nano-$FeS_2$@N-graphene cells with two other kinds of electrolytes were investigated and the cycling performances were shown in **Fig. S10**, further indicating that the ether-based electrolyte with $LiNO_3$ play a pivotal role in promoting the electrochemical stability.

The nano-$FeS_2$@N-graphene for Li-ion cells exhibit good rate capability shown in **Fig. 4a**. The reversible specific capacity is also very good with 768,

View Article Online
DOI: 10.1039/C5CC08002A




630, 484, 445, 391 and 285 mAh $g^{-1}$ at 0.05, 0.1, 0.5, 1, 2, 5 A $g^{-1}$ respectively, which then can be able to return to 475 mAh $g^{-1}$ at 0.5 A $g^{-1}$ (**Fig. 4b**). Compared to low conductive PAN matrix encapsulation[22], such $FeS_2$@N-graphene have high reversible capacity due to the formed continuous conductive paths by N-graphene frameworks among $FeS_2$ particles. What's more, long-term stability is one of key challenge for $FeS_2$ batteries. The Li-ion cells with core-shell $FeS_2$@N-graphene still own very high capacity (401.7 mAh $g^{-1}$) after 400 cycles at 0.5 A $g^{-1}$, corresponding to the specific energy of 637.1 Wh $kg^{-1}$. (in **Fig.4b**) Especially the coulombic efficiency of any cycle is very close to 100 %, attributing to the stable shell structure.

To further clarify reasons behind the good performance of core-shell nano-$FeS_2$@N-graphene, the AC-impediance meaurement is carried out to perform curves of 1st, 5th and 400th cycle at the discharged state (1.2~1.3 V) shown in **Fig. S11**. As is known, the semicircle at the high frequncy region is described to the charge transfer resistance ($R_{ct}$) at the cathode/electrolyte interface and the line region at the low area is ascribed to Li-ion diffusion. then, the values of $R_{ct}$ from the 1st to 5th cycle are changed from 10.5 to 12.2 Ω, and then to 400th cycle with about 61.4 Ω. Note that these results is much lower than those reported with $FeS_2$@C materials[14,15]. It's generally believed that the electrical conductivity influnces the $R_{ct}$ immensely. Hence, the big improvment of values of $R_{ct}$ in this work can be attributed to the N-graphene frameworks to be able to provide fast charge thransfer channels at the $FeS_2$/electrolyte interface to reduce the resistance. After long-term cycling, the $R_{ct}$ changes a little, meaning that the shell structure of nano-$FeS_2$@N-graphene is very stable.

Furthermore, for evaluating the practical value, we compare specific power-specific energy of core-shell nano-$FeS_2$@N-graphene to other commercial Li-ion battery cathodes, such as $LiCoO_2$, $LiFePO_4$, $LiMn_2O_4$, $LiNi_{0.5}Co_{0.2}Mn_{0.3}O_2$, etc.shown in **Fig.4c-d**. The advantage of nano-$FeS_2$@N-graphene is significant to have very high specific energy at different current (1275, 950, 713, 639, 543, 364 Wh $kg^{-1}$ at 0.05, 0.1, 0.5, 1, 2, 5 A $g^{-1}$ respectively), which is much higher than other commercial Li-ion cells cathodes (**Fig.4c**). Even compared to the reported pyrite $FeS_2$@C[21], the specific energy of core-shell $FeS_2$@N-graphene of this work is higher especially at high current rate area, further indicating the uniform and continuous N-graphene carbon frameworks can provide more continuous conductive paths between any prime $FeS_2$ particles. **Fig. 4d** shows the $FeS_2$@N-graphene to have stable cycle specific energy. Compared to the reported $LiCoO_2$ (~504 Wh $kg^{-1}$), $LiNi_{0.5}Co_{0.2}Mn_{0.3}O_2$ (~530 Wh $kg^{-1}$ at 0.5 A $g^{-1}$), $LiFePO_4$ (~450 Wh $kg^{-1}$ at 0.5 A $g^{-1}$) and $LiMn_2O_4$,(~390 Wh $kg^{-1}$ at 0.5 A $g^{-1}$), the $FeS_2$@N-graphene has a high energy density of 701 Wh $kg^{-1}$ after 100 cycles, whose specific energy retention is up to ~80%. Therefore, the $FeS_2$@N-graphene is a potential Li-ion cathode material for the next generation Li-ion batteries.

In summary, for solving the problems associated with the electroactive $FeS_2$ cathode species, a novel core-shell nano-$FeS_2$@N-graphene was prepared as a novel cathode material for Li-ion battery. Benifit of the amount of nanosize of $FeS_2$ nano-crystals as the core for Li-ion storage with high capacity and coated N-doped graphene as the shell with excellent electron conduction to enhance the structure stability, core-shell $FeS_2$@N-graphene exhibits more remarkable specific energy (950 Wh $kg^{-1}$ at 0.1 A $g^{-1}$) and higher specific power (543 Wh $kg^{-1}$ at 2.79 kW $g^{-1}$) than the commercial rechargeable LIB cathodes, as well as stable cycling performance. Hence $FeS_2$@N-graphene is proved to be a very promising candidate as a next generation advanced Li-ion cathode.

The research was financially supported by National Project for EV Batteries (20121110, OptimumNano, Shenzhen), Guangdong Innovation Team Project (No. 2013N080), and Shenzhen Science and Technology Research Grant(No. ZDSY20130331145131323, JCYJ20140903101633318).

## Notes and references

1 X. Xiao, X. Liu, L. Wang, H. Zhao, Z. Hu, X. He, Y. Li, Nano Research, 2012, **5**, 395.
2 Y.-L. Ding, J. Xie, G.-S. Cao, T.-J. Zhu, H.-M. Yu and X.-B. Zhao, Adv. Funct. Mater., 2011, **21**, 348.
3 C. Zhu, Y. Yu, L. Gu, K. Weichert and J. Maier, Angew. Chem., 2011, **50**, 6278.
4 Z. Wu, S. Ji, J. Zheng, Z. Hu, S. Xiao, Y. Wei, Z. Zhuo, Y. Lin, W. Yang, K. Xu, K. Amine and F. Pan, Nano lett., 2015, **15**, 5590.
5 T. A. Yersak, H. A. Macpherson, S. C. Kim, V.-D. Le, C. S. Kang, S.-B. Son, Y.-H. Kim, J. E. Trevey, K. H. Oh, C. Stoldt and S.-H. Lee, Adv. Energy Mater., 2013, **3**, 120.
6 P. J. Masset and R. A. Guidotti, J. Power Sources, 2008, **177**, 595.
7 D. Yichen, Z. Xiaoshu, Z. Xiaosi, H. Lingyun, D. Zhihui and B. Jianchun, J. Mater. Chem. A, 2015, **3**, 6787.
8 D. Yichen, Z. Xiaoshu, S. Ling, L. Yafei, Z. Xiaosi and B. Jianchun, J. Phys. Chem. C, 2015, **119**, 15874
9 J. Cabana, L. Monconduit, D. Larcher and M. R. Palacin, Adv. Mater., 2010, **22**, E170.
10 S. S. Zhang, J. Mater. Chem. A., 2015, **3**, 7689.
11 H. Xue, D. Y. W. Yu, J. Qing, X. Yang, J. Xu, Z. Li, M. Sun, W. Kang, Y. Tang and C.-S. Lee, J. Mater. Chem. A., 2015, **3**, 7945.
12 F. Rosamaria, J.R. Dahn and C. H. W. Jones, J. Electrochem. Soc., 1989, **136**, 3206.
13 A. Le Mehaute and A. Dugast, J. Power sources, 1983, **9**, 359.
14 D. Zhang, Y. J. Mai, J. Y. Xiang, X. H. Xia, Y. Q. Qiao and J. P. Tu, J. Power Sources, 2012, **217**, 229.
15 L. Liu, Z. Yuan, C. Qiu and J. Liu, Solid State Ionics, 2013, **241**, 25.
16 L. Li, M. Caban-Acevedo, S. N. Girard and S. Jin, Nanoscale, 2014, **6**, 2112.
17 V. Pelé, F. Flamary, L. Bourgeois, B. Pecquenard, F. Le Cras, Electrochem. Commun., 2015, **51**, 81.
18 T. Evans, D. M. Piper, S. C. Kim, S. S. Han, V. Bhat, K. H. Oh and S. H. Lee, Adv. Mater., 2014, **26**, 7386.
19 E. Strauss, J. Power Sources, 2003, **115**, 323.
20 A. Manthiram, Y. Fu, S. H. Chung, C. Zu and Y. S. Su, Chem. Reviews, 2014, **114**, 11751.
21 J. Liu, Y. Wen, Y. Wang, P. A. van Aken, J. Maier and Y. Yu, Adv. Mater., 2014, **26**, 6025.
22 S.-B. Son, T. A. Yersak, D. M. Piper, S. C. Kim, C. S. Kang, J. S. Cho, S.-S. Suh, Y.-U. Kim, K. H. Oh and S.-H. Lee, Adv. Energy Mater., 2014, 4, 1300961.
23 A. L. Reddy, A. Srivastava, S. R. Gowda, H. Gullapalli, M. Dubey and P. M. Ajayan, ACS nano 2010, **4**, 6337.
24 Z. S. Wu, W. Ren, L. Xu, F. Li and H. M. Cheng, ACS nano, 2011, **5**, 5463.
25 N. Mahmood, C. Zhang, F. Liu, J. Zhu and Y. Hou, ACS nano, 2013, **7**, 10307.
26 J. Hu, J. Zheng, L. Tian, Y. Duan, L. Lin, S. Cui, H. Peng, T. Liu, H. Guo, X. Wang and F. Pan, Chem. Commun., 2015, **51**, 7855.
27 Y. Wang, H. Sun, X. Duan, H. M. Ang, M. O. Tadé, S. Wang, Appl. Catal. B, 2015, **172-173**, 73.
28 W. Yang, X. Liu, X. Yue, J. Jia and S. Guo, J. Am. Chem. Soc., 2015, **137**, 1436.
29 S. Zhen, S. Lin, C. Jing, B. Wen, W. Feng and X. Xing, ACS nano, 2011, **5**, 4350.
30 Y. Zhang, W. J. Jiang, L. Guo, X. Zhang, J. S. Hu, Z. Wei and L. J. Wan, ACS Appl. Mater. interfaces, 2015, **7**, 11508.
31 Z. Sheng S, J. Electrochem. Soc., 2012, **159**, A920.
32 Z. Wang, C. Wu, L. Liu, J. Electrochem. Soc., 2002, **149**, A466.
33 E. Kendrick, J. Barker, J. Bao, A. Swiatek, J. Power sources, 2011, **196**, 6929;
34 R. Brec, E. Prouzet, G. Ouverard, J. Power Sources, 1989, **26**, 325.
35 C. Hongwei, W. Changhong, D. Weiling, L. Wei, D. Zhaolong, C. Liwei, Nano Lett., 2015, **15**, 798.